β, λ

Investigating the Combined Effect of Probabilistic Generation Forecasts and Dynamic Line Rating on Optimal Power Flow

Cheng Lyu, and Sara Eftekharnejad

Department of Electrical Engineering and Computer Science

Syracuse University, Syracuse, New York

David Larson
Electric Power Research Institute (EPRI)
Palo Alto, Califonia

Abstract-Current literature predominantly analyzes the effects of Variable Renewable Energy (VRE) forecasts on Optimal Power Flow (OPF) by presuming static line capacities, neglecting their variability with respect to temperature and wind speed. This study investigates the effect of probabilistic VRE forecasts on OPF, considering dynamic line rating (DLR) under scenarios of high VRE integration and variable weather conditions. Using various machine learning methods, VRE forecasts with different accuracy and prediction intervals (PIs) are generated. These forecasts are incorporated into a Monte Carlo-based probabilistic OPF (POPF) framework to evaluate the impact of probabilistic VRE forecasts on POPF, in contrast to OPF using actual generation data. Case studies using a modified IEEE 118-bus system demonstrate that while improvements in VRE forecast accuracy yield limited improvements to POPF reliability, DLR implementation significantly enhances OPF reliability.

Index Terms—Dynamic Line Rating, probabilistic renewable generation forecasts, probabilistic optimal power flow

NOMENCLATURE Solar absorptivity, and Air dynamic viscosity

 ϵ, δ, k_f Emissivity, Air density, and Air thermal conductivity ϕ, W Angle between wind and OHLs, and Wind speed (m/s) θ Effective incidence angle of solar ray A_p Conductor (OHLs) projected area C_r^1, C_r^0 Cost efficiencies of renewable generation C_s^2, C_s^1, C_s^0 Cost efficiencies of synchronous generations D Diameter of conductor (OHLs) N_l, N_d Number of transmission lines, and loads N_s, N_r Number of synchronous and renewable generations Q_d, P_d Reactive and active power of loads Q_l, P_l Reactive and active power loss on OHLs Q_r, P_r Reactive and active power of renewable generation Q_s, P_s Reactive and active power of conventional generation Q_{conv}, q_{se} Convective heat loss and solar radiation flux rates q_{rad}, q_{sun} Radiated heat loss rate, Heat gain rate from sun R_{T_c} AC resistance of conductor at temperature T_c

I. INTRODUCTION

Conductor temperature, Ambient air temperature (C°)

The increasing integration of VRE, and their inherent uncertainties, introduce novel challenges to power system operations and planning. Existing literature [1]–[6] shows that an accurate forecast of VRE can substantially address those challenges by mitigating the impacts of VRE uncertainties on power systems. Besides, extensive research [7]–[14] demonstrates

that DLR crucially influences OPF, and offers a robust solution to address the discrepancies arising from increased VRE integration levels. The thermal capacity limits of overhead lines (OHLs) are traditionally considered static, based on maximum-allowable conductor temperatures under ideal weather conditions. However, meteorological conditions are dynamic, often leading to enhanced conductor cooling effects and higher thermal capacities than those estimated using static line ratings (SLR). Consequently, utilizing VRE forecasts and DLR becomes essential in optimizing OPF. Studies analyzing the impact of VRE forecast accuracy and prediction intervals (PIs) on POPF considering DLR, especially under different weather scenarios, are absent in the existing literature. This gap signifies a lack of understanding regarding DLR's role in integrating probabilistic VRE forecasts into OPF analyses.

The Federal Energy Regulatory Commission (FERC)'s Order 881 underscores the benefits of DLR, advocating for further studies on its necessity in enhancing transmission reliability and security [15]. This paper aims to address the need for such studies by the following contributions:

- 1) Using probabilistic VRE forecasts from various Machine Learning (ML) models, the impact of VRE forecast accuracies and PI on POPF is investigated;
- 2) Investigated the combined impact of VRE forecasts and DLR on POPF for VRE penetration levels from 20% to 80%, using VRE data under diverse load conditions.

II. RELEVANT STUDIES

This section provides a comprehensive review of the state-of-the-art on how 1) VRE forecasts or 2) DLR enhances the efficiency and reliability of OPF. Recent studies have demonstrated that OPF models incorporating VRE uncertainty can enhance power system reliability. Specifically, a reversed accumulated percentage model was developed by authors in [1] to capture wind generation uncertainty on the IEEE 39-bus system. A parametric distribution OPF method designed in [2], integrating with analytical functions for optimal dispatch relative to renewable outputs, demonstrated superior computational and reliability performance compared to standard policies that linearly adjust control actions in response to system state changes and uncertainties. In another work [3], a quasi-Monte Carlo simulation (QMCS) with copula functions is developed to account for wind generation uncertainties in

POPF. The study in [4] introduces a day-ahead coordinated dispatch method for distribution networks, optimizing reactive power outputs of distributed generators (DGs) by using DG forecast errors. Additional studies on how VRE forecasts facilitate and improve OPF can be found in [5], [6].

The authors have previously demonstrated that incorporating DLR into OPF effectively reduces both line congestion and system costs [7]. In a similar work [8], a weather-based OPF model is developed by considering DLR, with case studies evidencing that DLR can maximize transmission capacity and reduce costs. DLR is also integrated with security constraint OPF (SCOPF) by authors in [9], proving that DLR can enhance system security and minimize the cost. In another work [10], DLR is combined with transmission switching to formulate an improved Linear AC OPF. Authors in [11] developed a constrained quadratic program method for the OPF problem considering DLR, which demonstrates that DLR increases system economic efficiency. In addition, DLR is integrated into a multi-period security-constrained OPF based on particle swarm optimization in [12]. Similar studies can be found in [13], [14], where DLR is integrated with OPF to produce an effective solution to improve system security and minimize operations costs.

The previous research efforts offer limited insights into the comprehensive impact of probabilistic VRE forecasts on POPF considering DLR. This study addresses this gap, rigorously evaluating the impact under scenarios of peak load, high VRE penetration, and varying weather conditions.

III. OPTIMAL POWER FLOW CONSIDERING DLR AND VRE FORECASTS

A. Dynamic Line Rating

DLR essentially adapts the current limit for OHLs based on environmental conditions, affecting their thermal capacity and the maximum power transmission capability [8]. The DLR of OHLs can be calculated based on IEEE Standard 738-2006 [16], which provides the heat balance equation for OHLs:

$$q_{conv} + q_{rad} = q_{sun} + p_{loss} \tag{1}$$

Given $p_{loss} = I^2 R_{T_c}$, the current flowing in OHLs can be obtained as [16]:

$$I = \sqrt{\frac{q_{conv} + q_{rad} - q_{sun}}{R_{T_c}}} \tag{2}$$

where
$$q_{sun} = \beta q_{se} sin(\theta) A_p$$
; $A_p = Dcos(\theta)$
 $q_{rad} = 0.0178 \times D\epsilon \left[\frac{(T_c + 273)^4}{100} - \frac{(T_a + 273)^4}{100} \right]$ (3)

The forced convection heat loss rate [16], $q_{conv} =$

$$\begin{cases}
[0.0119 \left(\frac{D\delta W}{\lambda}\right)^{0.6}] k_f K_a (T_c - T_a) &, W \leq 4.47 \\
[1.01 + 0.0372 \left(\frac{D\delta W}{\lambda}\right)^{0.52}] k_f K_a (T_c - T_a) &, W > 4.47
\end{cases}$$
(4)

where $K_a = 1.194 - \cos(\phi) + 0.194 \times \cos(2\phi) + 0.368 \times 0.000$ $\sin(2\phi)$. Upon substituting (3) and (4) into (2), the current in OHLs can be articulated as a function of meteorological parameters T_a, W, θ, ϕ . In this work, OHL midpoints are chosen for GPS coordinates to obtain meteorological data such as temperature, wind speed, wind direction, and zenith angle. Specifically, θ is set as equal to the zenith angle, and ϕ denotes the angle difference between wind speed and line direction. The benchmark I_{SLR} from SLR is ascertained at $T_a = 40(C^{\circ}), T_c = 80(C^{\circ}),$ and wind speed of zero [17]. The time-varying I_{DLR} is derived from forecasted meteorological data for each line, thereby modulating the thermal capacity for each line based on prevailing weather conditions.

B. Probabilistic VRE Forecasts using ML methods

Recent literature highlights ML as the primary method for VRE forecast, with foundational studies outlined in [18]-[21]. This research critically examines probabilistic forecasting models developed based on 1) Persistence Ensemble (PeEn), 2) Quantile Regression (QR), 3) Feed Forward Neural Networks (FFNN), and 4) Long Short-Term Memory networks (LSTM), to generate probabilistic predictions in VRE output.

- 1) Persistence Ensemble (PeEn): In this study, the probabilistic PeEn model leverages historical data at hour t for future predictions at the same hour. Denoting y_t as the observed value at hour t, historical data for this hour is aggregated to construct a distribution function $f_t(y)$, which is applied to provide probabilistic forecasts for hour t.
- 2) Quantile Regression (QR): The τ -th quantile estimated by the QR method is denoted as $\hat{y}_{\tau} = x^T \hat{\alpha}(\tau)$. To consider the non-linear nature of meteorological variables, each meteorological variable x is first converted to polynomial format: $x_{poly} = [x, x^2]$. For each specified quantile τ , the QR seeks to minimize the sum of asymmetrically weighted absolute residuals. The solution for the τ -th quantile [22] is:

$$\alpha(\tau) = \underset{\alpha}{\operatorname{argmin}} \sum_{i=1}^{n} \rho_{\tau}(\tau) \left(y_{i} - \mathbf{x}_{\text{poly},i}^{T} \boldsymbol{\alpha}(\tau) \right)$$
 (5)

where $\rho_{\tau}(u) = u(\tau - 1)$ if (u < 0) or $\rho_{\tau}(u) = u\tau$ if (u < 0), and $u = y_i - \mathbf{x}_{\text{poly,i}}^T \boldsymbol{\alpha}(\tau)$

3) Feed Forward Neural Networks (FFNN): In this study, the FFNN is structured specifically to yield probabilistic forecasts by estimating the parameters of a predefined Normal distribution, $N(\mu, \sigma^2)$. The implemented FFNN architecture incorporates two distinct nodes within its dense layer, dedicated separately to predicting the mean (μ) and standard deviation (σ) of the distribution. Given the predicted distribution and observations y, the loss function for training the FFNN is the negative log-likelihood of the observed data:

$$\mathcal{L} = -\sum \log N(y_i|\mu_i, \sigma_i^2) \tag{6}$$

4) Long Short-Term Memory networks (LSTM): LSTM is a specialized kind of Recurrent Neural Network (RNN) that is distinguished by its unique structure comprising memory cells, input gates, output gates, and forget gates [23]. In this work, the output is predefined as Normally distributed, and the two nodes in the LSTM dense layer predict the mean (μ) and standard deviation (σ).

C. Probabilistic OPF based on Monte Carlo Method

Given the obtained distribution of VRE generation forecasts using methods discussed in Section III-B, MC simulation is applied to generate random samples from these distributions. For each set of random samples, a deterministic OPF is formulated to minimize generation costs while maintaining generation-load balance and adhering to safety constraints. The objective function of the OPF is expressed as:

minimize
$$\sum_{i=1}^{N_s} (C_{s_i}^2 P_{s_i}^2 + C_{s_i}^1 P_{s_i} + C_{s_i}^0) + \sum_{i=1}^{N_r} (C_{r_i}^1 P_{r_i} + C_{r_i}^0) \text{ high temperature) and a summer off-peak day (Jul 2nd-rain in several regions). The developed QR, FFNN, and LSTM$$

Subject to
$$\sum_{i=1}^{N_s} Q_{s_i} + \sum_{i=1}^{N_r} Q_{r_i} = \sum_{i=1}^{N_l} Q_{l_i} + \sum_{i=1}^{N_d} Q_{d_i}$$
 (8)

$$\sum_{i=1}^{N_s} P_{s_i} + \sum_{i=1}^{N_r} P_{r_i} = \sum_{i=1}^{N_l} P_{l_i} + \sum_{i=1}^{N_d} P_{d_i}$$
 (9)

$$P_{s_i,min} \le P_{s_i} \le P_{s_i,max} \tag{10}$$

$$Q_{s_i,min} \le Q_{s_i} \le Q_{s_i,max} \tag{11}$$

$$P_{r_i} \le P_{r_i,max} \tag{12}$$

$$V_{i,min} \le V_i \le V_{i,max} \tag{13}$$

$$L_i \le L_{i,max} \tag{14}$$

Eq. (7) breaks down the cost into two parts: the cost from the conventional generation and the cost from VRE. Eq. (8) and (9) define the active and reactive power balance constraints, (10) and (11) set the active and reactive power limits for conventional generators, and (12) sets the maximum power output for VRE. MC samples of VRE forecasts are used to adjust the maximum power values $P_{r_i,max}$. Bus voltage limits are expressed in (13), setting the upper and lower limits at 1.05 and 0.95 per unit, respectively. The DLR is included in the OPF analysis by changing OHLs capacity limits $L_{i,max}$.

The deterministic OPF is repeated numerous times until further increasing the sample size would not change the results significantly. To balance the effectiveness of results and running time, the sample size is tested and set as 1,000 for the case studies introduced in the next section. Given line loading L_i as an example, the POPF results are thus obtained using the empirical probability distribution function (EPDF):

$$f_{L_i}(l) = \frac{1}{dL} \cdot \frac{1}{n} \sum_{i=1}^n \mathbf{1} \{ L_{li} \le L \} d(L)$$
 (15)

IV. CASE STUDIES

A. A Modified IEEE 118-bus Case and Data Description

The POPF methodologies were evaluated using a modified IEEE 118-bus system [24] with 181 lines, 99 loads, 8 solar generators, 6 wind generators, 30 synchronous generators, and a slack bus. Real load and VRE data for summer 2023 were sourced from ERCOT's 60-Day SCED Disclosure Reports [25] and adjusted to fit the modified system. The layout of load and VRE is modeled based on their real-world locations. Notably, the spatial arrangement of solar and wind generation sites were

intentionally separated, based on their geographic coordinates, to mitigate any potential correlation in the output of different VREs. Meteorological data used to train forecasting models and estimate the DLR of OHLs is derived from the High-Resolution Rapid Refresh (HRRR) model [26]. The variables derived for training include temperature, relative humidity, dew points, wind speed, wind degree, wind gusts, air pressure, cloud cover, and zenith angle. Two case studies were conducted: a summer peak-load day (Aug 11th- sunny and high temperature) and a summer off-peak day (Jul 2nd-rain in several regions). The developed QR, FFNN, and LSTM models are trained using the previous two months of test data. The PeEn model was trained using the previous week's data as it tends to be more accurate than those using more data.

B. Evaluation Criteria

To assess the impact of probabilistic VRE on POPF, a comparison is drawn between the OPF utilizing real generation data and the POPF using VRE forecasts, both with and without DLR. Real load data are used for all scenarios. The deviation between VRE predictions and actual outputs, as well as the discrepancy between real OPF results and the POPF using forecasts, is measured using the normalized Continuous Ranked Probability Score (nCRPS) (16):

$$nCRPS(F, y) = \frac{1}{y_{max}} \int_{-\infty}^{\infty} (F(\hat{y}) - \mathbf{1}_{y \le \hat{y}})^2 d\hat{y} \times 100\%$$
 (16)

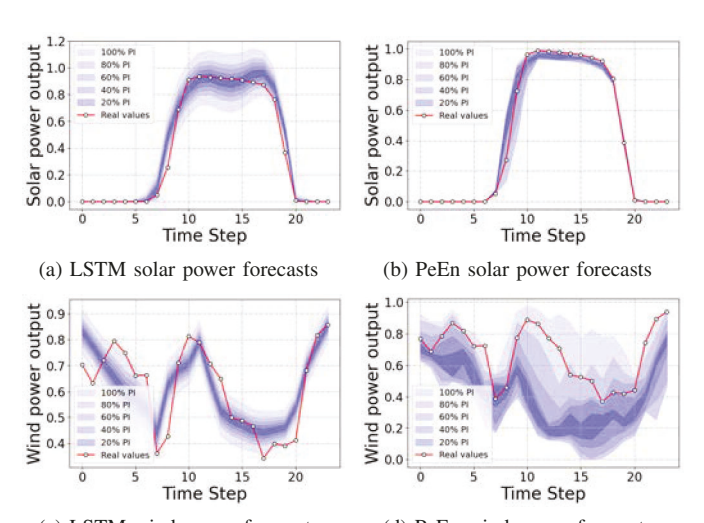
C. Day-ahead Probabilistic VRE forecasts

For the summer peak day, VREs generated more power compared to the off-peak day. This difference is mainly due to heavy rains during the off-peak day. In each scenario, this study tests four VRE penetration levels: 20%, 40%, 60%, and 80%. The study does not concentrate on optimizing the locations of VREs; rather, higher VRE penetration ratios are simulated by enhancing the capacity of existing VRE facilities.

Day-ahead VRE forecasts utilizing the PeEn, QR, FFNN, and LSTM models are detailed in Table I, where "Solar" is the mean nCRPS from eight solar generation forecasts, "Wind" is the mean nCRPS for six wind generation forecasts, and the "Mean" is the average nCRPS of all VREs. The values in Table I are calculated using normalized VRE outputs, i.e., dividing each by its maximum output. This implies that minor errors in normalized forecasts become larger when the forecasts are rescaled to their original values, particularly impacting POPF analyses in high VRE penetration scenarios.

					Summer off-peak-load day			
	PeEn	QR	FFNN	LSTM	PeEn	QR	FFNN	LSTM
Solar (%)	2.2	5.5	6.4	5.7	10	16.8	13.6	7.3
Wind (%)	11	8.2	7.5	6.4	24	15	10.1	8.5
Mean (%)	5.9	6.7	6.9				12.1	7.8

Table I indicates that LSTM generally outperforms other models in forecast accuracy. Rainy conditions reduce off-peak load day forecast accuracy compared to peak day forecasts. This study extends beyond a general evaluation of the impact of various VRE forecasts on POPF by also making two key comparisons. Firstly, Fig. 1 shows the comparison of LSTM and PeEn forecasts for the peak-load day. Despite their similar overall forecast accuracy (Table I), notable differences exist in their solar and wind forecast accuracies, with PeEn outperforming LSTM in solar but lagging in wind forecast. This comparison aims to discern whether solar or wind power forecasts have a more significant influence on POPF. Secondly, Fig. 2 illustrates forecasts from the FFNN and QR models for the off-peak day. While the FFNN model shows higher accuracy than the QR model (Table I), the QR model's forecasts exhibit a narrower PI. This comparative analysis is employed to evaluate how the forecast PI impacts POPF.



(c) LSTM wind power forecasts (d) PeEn wind power forecasts Fig. 1. Comparing LSTM and PeEn Forecasts for Summer Peak Load Day

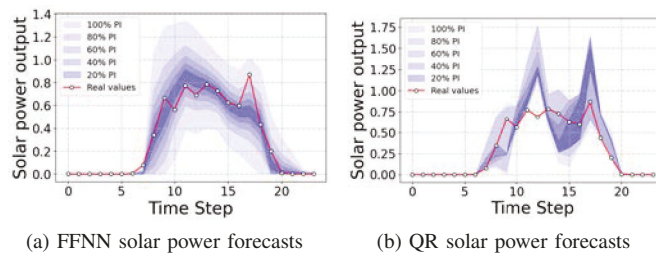


Fig. 2. Comparing FFNN and QR Forecasts for Summer Off Peak Load Day

D. POPF using VRE forecasts without DLR

The day-ahead POPF with VRE forecasts is compared with OPF using actual VRE data. The precision of the day-ahead POPF is analyzed by quantifying the discrepancy in line loadings across all lines and comparing results from the OPF using actual generation data with those using VRE forecasts. $nCRPS^*$ in Table II presents the hourly average nCRPS for line loadings across all lines. The values are computed as the hourly mean of nCRPS for each line loading, which is the average nCRPS across all lines for each hour.

$$nCRPS^* = \frac{1}{N_l} \sum_{i=1}^{N_l} * \frac{1}{24} \sum_{j=1}^{24} nCRPS_{i,j}$$
 (17)

A higher value indicates greater deviations between POPF line flows and OPF results using actual VRE.

TABLE II $nCRPS^st$ for line loadings from day-ahead POPF without DLR

POPF	Sui	nmer j	eak-load	l day	Summer off-peak-load day				
with	PeEn	QR	FFNN	LSTM	PeEn	QR	FFNN	LSTM	
20%*	2.69	2.66	2.66	2.62	1.63	1.62	1.69	1.55	
40%*	4.71	4.64	4.64	4.54	2.39	2.28	2.47	2.17	
60%*	6.58	6.5	6.49	6.36	3.25	3.06	3.28	2.94	
80%*	8.23	8.06	8.1	7.9	4.13	3.93	4.12	3.75	

*20%, 40%,60%, and 80% refer to VRE penetration ratio of the system

Based on Table II, improved accuracy in VRE forecasts leads to more reliable POPF. However, the gains from improved forecast accuracy are limited. For example, a notable improvement in LSTM and PeEn forecast accuracy for an offpeak day (nCRPS reduced from 16.2% to 7.8%) leads to only a slight reduction in line flow error in 80% VRE penetration scenarios (from 4.13% to 3.75%). Moreover, compared to the peak day, the POPF shows greater reliability on off-peak days due to smaller deviations in line loadings, even though VRE forecasts are less precise during the day. This is due to the reduced demand volatility inherent to off-peak days.

For the first comparison discussed earlier, POPF with LSTM forecasts yields higher precision than that with PeEn for peak days, suggesting that precise wind generation forecasts are more crucial for POPF accuracy than solar generation forecasts. The second comparison offers further insights. Despite the higher accuracy of FFNN forecasts compared to QR for an off-peak day, POPF utilizing QR forecasts is more precise. This indicates that narrower PIs with fairly accurate VRE forecasts enhance POPF reliability more effectively than higher-accuracy forecasts with wider PIs. This could be due to the impact of tail events on POPF, in VRE forecasts with broader PIs, potentially compromising its reliability.

E. POPF using VRE forecasts with DLR

In addition to forecasts, this section integrates DLR into the POPF to evaluate the effect of probabilistic VRE forecasts in conjunction with DLR. As outlined in Section IV-A, the DLR for POPF utilizes data from the HRRR model, while the DLR for the baseline OPF is based on reanalysis data from the ERA5 model [27]. It is important to note that the primary focus of this research is not on the precision of DLR in OPF, but rather on comparing the performance of POPF with forecast data against OPF with real data.

Based on Table III, the inclusion of DLR enhances the reliability of POPF. This enhancement is more pronounced than the improvements by refining ML-based forecast models. Even the simpler PeEn VRE forecast model, when combined with DLR, leads to more dependable POPF outcomes compared to using advanced LSTM forecasts alone. Furthermore, DLR tends to amplify the positive impact of accurate VRE forecasts on POPF, suggesting that DLR results in more reliable POPF when coupled with precise VRE output predictions.

Fig. 3 shows the comparative analysis of POPF performance with VRE forecasts and DLR integration at varied VRE pen-

Γ	POPF	Summer peak-load day				Summer off-peak-load day			
L	with	PeEn	QR	FFNN	LSTM	PeEn	QR	FFNN	LSTM
Ī	20%*	2.32	2.26	2.29	2.2	1.58	1.58	1.63	1.5
İ	40%*	3.88	3.75	3.84					1.96
İ	60%*	5.24	5.1	5.17	4.97	2.76	2.62	2.82	2.54
	80%*	6.82	6.6	6.71		3.46	3.34	3.50	3.23

*20%, 40%,60%, and 80% refer to VRE penetration ratio of the system

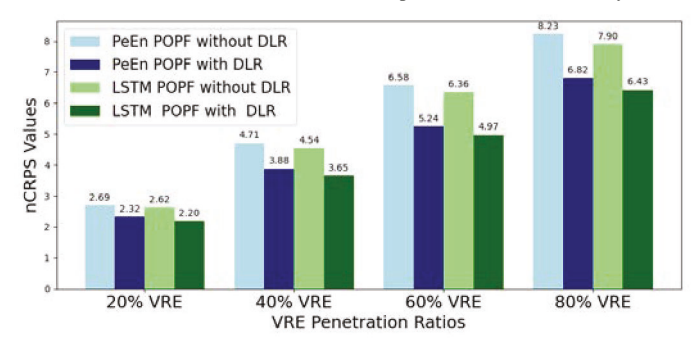


Fig. 3. Comparative Analysis of POPF Performance

etration ratios. Notably, a simple PeEn forecast model, when coupled with DLR, provides more reliable POPF outcomes than those sorely using a sophisticated LSTM forecast.

V. CONCLUSION

This study examines the effect of VRE forecasts on POPF considering DLR. Various ML-based probabilistic VRE forecast methods, such as LSTM, FFNN, QR, and PeEn, are considered. By comparing day-ahead POPFs that employ different VRE forecasts using actual historical generation data, the study assesses the improvement in POPF precision resulting from advancements in VRE forecast accuracy and applying DLR.

Case studies on a modified IEEE 118-bus system show that the inclusion of DLR significantly enhances the reliability of POPF results. This enhancement indicates that while increasing the accuracy of VRE forecasts contributes to a more reliable POPF, incorporating DLR can further amplify this effect. The study also notes the impact of forecast PIs on POPF: wider PIs, due to the potential for significant tail events, may reduce POPF reliability. The case studies also underline that accurate wind power forecasts are more influential than solar power forecasts in enhancing POPF reliability.

Future research can investigate the potential role of more reliable computing methodologies in mitigating the adverse effects of forecasting errors. Such research could investigate how advanced computational strategies and robust optimization models can enhance the resilience and reliability of POPF outcomes in the face of forecast inaccuracies.

REFERENCES

- S. Albatran, S. Harasis, M. Ialomoush, Y. Alsmadi, and M. Awawdeh, "Realistic optimal power flow of a wind-connected power system with enhanced wind speed model," *IEEE Access*, vol. 8, 2020.
- [2] Z. Guo, W. Wei, L. Chen, Z. Dong, and S. Mei, "Parametric distribution optimal power flow with variable renewable generation," *IEEE Trans.* on Power Systems, vol. 37, no. 3, pp. 1831–1841, 2021.

- [3] Z. Xie, T. Ji, M. Li, and Q. Wu, "Quasi-monte carlo based probabilistic optimal power flow considering the correlation of wind speeds using copula function," *IEEE Trans. on Power Systems*, vol. 33, no. 2, 2017.
- [4] L. Zhang, W. Tang, J. Liang, P. Cong, and Y. Cai, "Coordinated dayahead reactive power dispatch in distribution network based on real power forecast errors," *IEEE Trans. on Power Systems*, 2015.
- [5] R. Entriken, A. Tuohy, and D. Brooks, "Stochastic optimal power flow in systems with wind power," in 2011 IEEE Power and Energy Society General Meeting, 2011, pp. 1–5.
- [6] Y. Sun, Y. Guo, R. Mao, and S. M. Malik, "A wind forecast error cost included OPF model and its fast algorithm," in 2014 IEEE PES General Meeting— Conference & Exposition, 2014, pp. 1–5.
- [7] C. Lyu and S. Eftekharnejad, "The impacts of dynamic line rating on systems with high levels of renewable energy resources," in 2023 IEEE Power & Energy Society General Meeting (PESGM), 2023, pp. 1–5.
- [8] J. Cao, W. Du, and H. Wang, "Weather-based optimal power flow with wind farms integration," *IEEE Trans. on Power Systems*, 2015.
- [9] S. Triwijaya, N. Sugiantoro, Y. Prasetyo, R. S. Wibowo, O. Penangsang et al., "Security constrained optimal power flow considering dynamic line rating," in 2018 10th International Conference on Information Technology and Electrical Engineering (ICITEE), 2018, pp. 46–51.
- [10] M. A. Mohamed, E. M. Awwad, A. M. El-Sherbeeny, E. A. Nasr, and Z. M. Ali, "Optimal scheduling of reconfigurable grids considering dynamic line rating constraint," *IET Generation, Transmission & Distribution*, vol. 14, no. 10, pp. 1862–1871, 2020.
- [11] N. Sugiantoro, R. S. Wibowo, V. Lystianingrum, E. Rovianto, and S. Triwijaya, "Optimal power flow with dynamic line rating using quadratically constrained quadratic program method," in 2021 1st International Conference on Electronic and Electrical Engineering and Intelligent System (ICE3IS), 2021, pp. 54–59.
- [12] A. A. E. Hamed, S. M. Abdelkader, and A. A. Eladl, "Integrating dynamic line rating in security constrained optimal power flow considering wind power generation," MEJ. Mansoura Engineering Journal, 2020.
- [13] M. Nick, O. A. Mousavi, R. Cherkaoui, and M. Paolone, "Integration of transmission lines dynamic thermal rating into real-time optimal dispatching of power systems," in 2015 50th International Universities Power Engineering Conference (UPEC), 2015, pp. 1–6.
- [14] D. Fang, M. Zou, and S. Djokic, "Probabilistic OPF incorporating uncertainties in wind power outputs and line thermal ratings," in 2018 IEEE International Conference on Probabilistic Methods Applied to Power Systems (PMAPS), 2018, pp. 1–6.
- [15] "FERC Docket No. AD22-5, order 881," 2022. [Online]. Available: https://www.ferc.gov/media/ad22-5-000
- [16] "IEEE standard for calculating the current-temperature of bare overhead conductors," IEEE Std 738-2006 (Revision of IEEE Std 738-1993), 2007.
- [17] International Renewable Energy Agency, "Dynamic line rating: Innovation landscape brief," 2020.
- [18] C. Lyu, S. Basumallik, S. Eftekharnejad, and C. Xu, "A data-driven solar irradiance forecasting model with minimum data," in 2021 IEEE Texas Power and Energy Conference (TPEC), 2021, pp. 1–6.
- [19] C. Lyu, S. Eftekharnejad, S. Basumallik, and C. Xu, "Dynamic feature selection for solar irradiance forecasting based on deep reinforcement learning," *IEEE Trans. on Industry Applications*, vol. 59, no. 1, 2022.
- [20] D. P. Larson, L. Nonnenmacher, and C. F. Coimbra, "Day-ahead fore-casting of solar power output from photovoltaic plants in the american southwest," *Renewable Energy*, vol. 91, pp. 11–20, 2016.
- [21] D. P. Larson and C. F. Coimbra, "Direct power output forecasts from remote sensing image processing," *Journal of solar energy engineering*, vol. 140, no. 2, p. 021011, 2018.
- [22] P. Lauret, M. David, and H. T. Pedro, "Probabilistic solar forecasting using quantile regression models," *energies*, vol. 10, no. 10, 2017.
- [23] V. Suresh, F. Aksan, and et al, "Probabilistic Istm-autoencoder based hour-ahead solar power forecasting model for intra-day electricity market participation: A polish case study," *IEEE Access*, 2022.
- [24] C. Lyu, "A modified IEEE 118-bus system with time series data," 2023. [Online]. Available: https://dx.doi.org/10.21227/dafq-e974
- [25] "60-day sced disclosure reports." [Online]. Available: https://www.ercot.com/mp/data-products/data-product-details?id=NP3-965-ER
- [26] "High-resolution rapid refresh (HRRR)." [Online]. Available: https://rapidrefresh.noaa.gov/hrrr/
- [27] H. Hersbach, B. Bell, P. Berrisford, S. Hirahara, A. Horányi, J. Muñoz-Sabater, J. Nicolas, C. Peubey, R. Radu, D. Schepers et al., "The era5 global reanalysis," *Quarterly Journal of the Royal Meteorological Society*, vol. 146, no. 730, pp. 1999–2049, 2020.